An Automated Brightband Height Detection Algorithm for Use with Doppler Radar Spectral Moments

ALLEN B. WHITE AND DANIEL J. GOTTAS

Cooperative Institute for Research in Environmental Sciences, NOAA/Environmental Technology Laboratory, University of Colorado, Boulder, Colorado

ERIC T. STREM

NOAA/National Weather Service, California–Nevada River Forecast Center, Sacramento, California

F. MARTIN RALPH AND PAUL J. NEIMAN

NOAA/Environmental Technology Laboratory, Boulder, Colorado

(Manuscript received 28 May 2001, in final form 7 October 2001)

ABSTRACT

Because knowledge of the melting level is critical to river forecasters and other users, an objective algorithm to detect the brightband height from profiles of radar reflectivity and Doppler vertical velocity collected with a Doppler wind profiling radar is presented. The algorithm uses vertical profiles to detect the bottom portion of the bright band, where vertical gradients of radar reflectivity and Doppler vertical velocity are negatively correlated. A search is then performed to find the peak radar reflectivity above this feature, and the brightband height is assigned to the altitude of the peak. Reflectivity profiles from the off-vertical beams produced when the radar is in the Doppler beam swinging mode provide additional brightband measurements. A consensus test is applied to subhourly values to produce a quality-controlled, hourly averaged brightband height. A comparison of radar-deduced brightband heights with melting levels derived from temperature profiles measured with rawinsondes launched from the same radar site shows that the brightband height is, on average, 192 m lower than the melting level. A method for implementing the algorithm and making the results available to the public in near–real time via the Internet is described. The importance of melting level information in hydrological prediction is illustrated using the NWS operational river forecast model applied to mountainous watersheds in California. It is shown that a 2000-ft increase in the melting level can triple run off during a modest 24-h rainfall event. The ability to monitor the brightband height is likely to aid in melting-level forecasting and verification.

1. Introduction

The *bright band* (BB) is a layer of enhanced radar reflectivity resulting from the difference in the dielectric factor for ice and water and the aggregation of ice particles as they descend and melt. The *brightband height* (BBH) is the altitude of maximum radar reflectivity in the BB. The layer over which the transformation from ice to water occurs defines the *melting layer*. The top of the melting layer is the *melting level*, also commonly accepted as the altitude of the 0°C constant-temperature surface (Glickman 2000). Knowledge of the melting layer is extremely useful to the weather forecast community, for example, to predict and monitor the *snow level*, defined here as the lowest level in the atmosphere where snow or ice completely changes to rain (as opposed to the surface elevation where snow or ice accumulates on the ground). Other potential users include road maintenance crews, hydrologists, emergency managers, electric utilities, aviators, and the ski industry. The snow level coincides with the bottom of the melting layer. However, we are unaware of direct or indirect measurement techniques capable of providing this information on a routine basis. The BBH can be measured directly and routinely using Doppler radar and provides a better estimate of the snow level than the melting level because of the time required for snow to melt at temperatures above freezing.

During the Pacific Land-falling Jets Experiment (PACJET; January–March 2001; more information available online at http://www.etl.noaa.gov/programs/pacjet/), an automated algorithm to detect the BBH using profiles of radar reflectivity and Doppler vertical velocity (DVV) was field tested at two northern California wind profiler sites (see Fig. 1). At Bodega Bay, California (BBY), a melting level verification dataset was also obtained by

Corresponding author address: Dr. Allen B. White, NOAA/ETL/R/ET7, 325 Broadway, Boulder, CO 80305.
E-mail: allen.b.white@noaa.gov

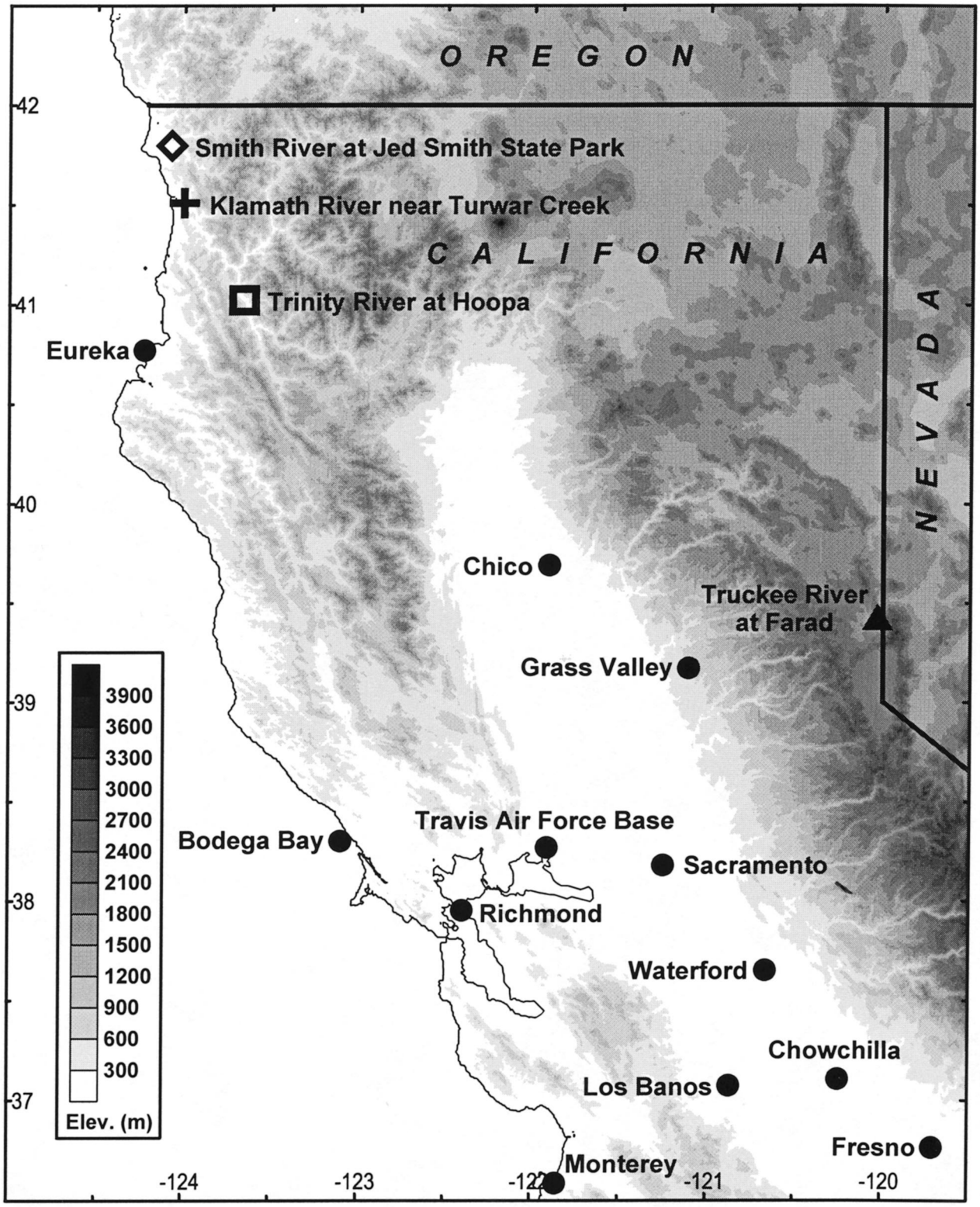

FIG. 1. Base map of central and northern California showing the locations of 915-MHz wind profilers (dots) deployed during PACJET. The wind profiler at Monterey was provided by the Naval Postgraduate School. The wind profiler at Travis Air Force Base was provided by the U.S. Air Force. During PACJET, the BBH detection scheme described in this paper was in operation at Bodega Bay and Grass Valley, California. River basins used to show the sensitivity of runoff to changes in melting level (see section 2) are indicated by the noncircular symbols.

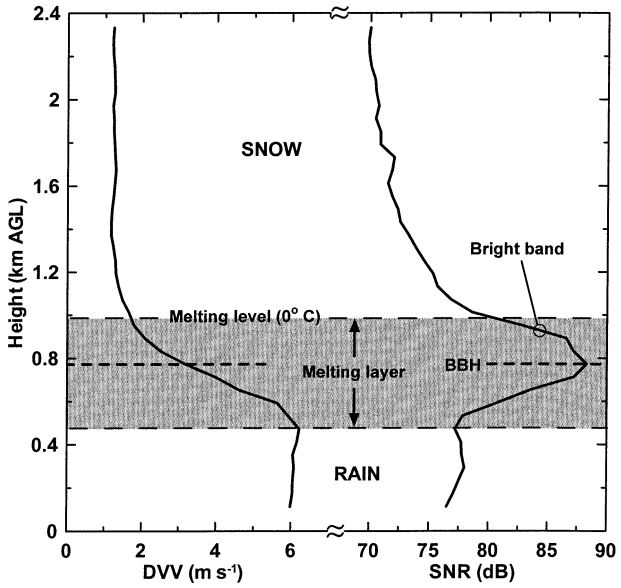

FIG. 2. Hourly median profiles of radar reflectivity, in the form of range corrected SNR, and DVV (positive downward) measured with the vertical beam of the 915-MHz wind profiler at Bodega Bay, California, between 1100 and 1200 UTC on 24 Feb 2001. The BBH is indicated by the bold dashed line at 0.772 km AGL. The melting level or melting-layer top measured by a rawinsonde launched from Bodega Bay at 1126 UTC is shown by the dashed line at 0.994 km AGL. For illustration, the bottom of the melting layer is estimated to be at the bottom of the bright band, which is also where DVV is largest. The profiles were measured in stratiform rain during a period of decreasing BBH (see Fig. 7).

launching serial rawinsondes during the period 23 January–25 February 2001. This paper describes the automated BBH detection algorithm and the technique used during PACJET to make the output from this algorithm available on the internet in near–real time. The remainder of this section explains our motivation for using profiles of DVV in addition to radar reflectivity to detect the bright band. Section 2 shows how accurate information about the melting level is critical to the success of operational river forecasts, providing an example of a user community who could benefit from real-time measurements of BBH. Section 3 describes the physical characteristics of the bright band that make the detection algorithm possible. Section 4 provides a detailed description of the BBH detection algorithm and includes a comparison of brightband heights determined by the algorithm with melting levels measured with rawinsondes during PACJET. Section 5 describes methods for accessing wind profiler data from the data acquisition file archive and making brightband measurements available to the public in a timely manner.

Figure 2 shows the behavior of vertical profiles of radar reflectivity and DVV obtained in rain containing a BB. Since the BB coincides with an often sharp radar reflectivity enhancement, one choice for BBH detection would be to search only the radar reflectivity profile for this enhancement. BBH detection using volumetric radar reflectivity measurements from Next Generation Weather Radar (NEXRAD) has recently been proposed (Burrows 2001; Gourley et al. 2001). Scanning Doppler radars, like NEXRAD, can be configured to provide vertical profiles of DVV. Unfortunately, the highest elevation scan established for NEXRAD operating in the default precipitation mode is 19.5°. The National Oceanic and Atmospheric Administration (NOAA) National Severe Storms Laboratory used a vertically pointing Doppler S-band radar to verify BBHs detected by NEXRAD (Gourley 2001, personal communication). Fabry and Zawadzki (1995) used a vertically pointing X-band radar for BBH detection. However, this radar did not provide velocity data. The potential risk of using only radar reflectivity for BBH detection is that, depending on the radar's wavelength, reflectivity enhancements can result from features other than the BB. Examples include clear-air turbulence, the boundary layer top, and clouds, as well as forms of stationary and intermittent clutter targets (e.g., Wilczak et al. 1995; White et al. 1996).

To narrow the search of the profile to the height region where the BB exists, our method uses both radar reflectivity and DVV profiles to detect the bottom portion of the BB, where vertical gradients of radar reflectivity and DVV are negatively correlated. A search is then performed to find the peak radar reflectivity above this feature, and the BBH is assigned to the altitude of this peak. The use of DVV in addition to radar reflectivity gives added confidence to BBH detection while also allowing for detection when the precipitation does not reach the surface or is too light to produce a definitive BB in only the radar reflectivity profile (Smith 1983). The basic technique described here can be used with any atmospheric profiling Doppler radar with an operating frequency that is sensitive to hydrometeors but that does not suffer severe attenuation in rainfall. The method is applicable, then, to radars operating in the frequency range of roughly 400–4000 MHz. One example is the commercially available 915-MHz Doppler wind profiler (Ecklund et al. 1988), which is the instrument used here to demonstrate the algorithm.

2. Sensitivity of simulated runoff to changes in melting level

One area of operational forecasting that could realize a substantial benefit from real-time BBH measurements is river forecasting. River forecasters rely on forecasts of the melting level and quantitative precipitation to help predict runoff in mountainous terrain. Typically, this information is provided by a coarsely resolved, both in time and space, weather forecast model. Strategically placed wind profilers could provide highly resolved (hourly temporal resolution, 100-m vertical resolution) BBH measurements for real-time melting-level forecast verification for basins located near the wind profiler and more accurate melting-level forecasts for basins located downstream of the wind profiler. This section presents

TABLE 1. California river basins used in the NWSRFS model runs.

River/basin	Basin area (mi^2)	Response time* (h)	Monitor/ flood stage (ft)	Monitor/ flood flow (cfs $\times 10^{-3}$)	MAP** (in.)
Klamath River near Turwar Creek	772	18	NA	NA	69.5
Smith River at Jedediah Smith State Park	614	6	25/29	76.2/117.7	102.5
Trinity River at Hoopa	650	18	44/48	129.3/157.5	62.6
Truckee River at Farad	204	6	10/11	8.64/10.5	41.1

* Response time = peak ordinate of the 6-h unit hydrograph.
** MAP= basin mean annual precipitation.

hydrological modeling results that demonstrate the acute sensitivity of runoff to changes in the melting level.

The California Nevada River Forecast Center (CNRFC) of the National Weather Service uses the National Weather Service River Forecast System (NWSRFS) for real-time river forecasting. The NWSRFS is a collection of modules or operations that can be selected to perform various hydrologic forecasting procedures (Smith and Page 1993). The two operations that were used in this analysis are the snow accumulation and ablation model, SNOW-17, developed at the Hydrologic Research Laboratory of the Office of Hydrology (Anderson 1973) and the Sacramento Soil Moisture Accounting Model (SAC-SMA) developed by at the CNRFC (Burnash et al. 1973).

SNOW-17 is a conceptually based model in which each of the significant physical processes affecting snow accumulation and snowmelt are parameterized. Also included in this operation is an area elevation curve for the basin being simulated. The area elevation curve gives the percentage of the basin below a specified altitude and is generated using a Geographic Information Software application. Given forecasts of melting level, temperature, and precipitation, SNOW-17 will determine the distribution of snow and rain plus melt over the basin. The output of SNOW-17 drives the SAC-SMA.

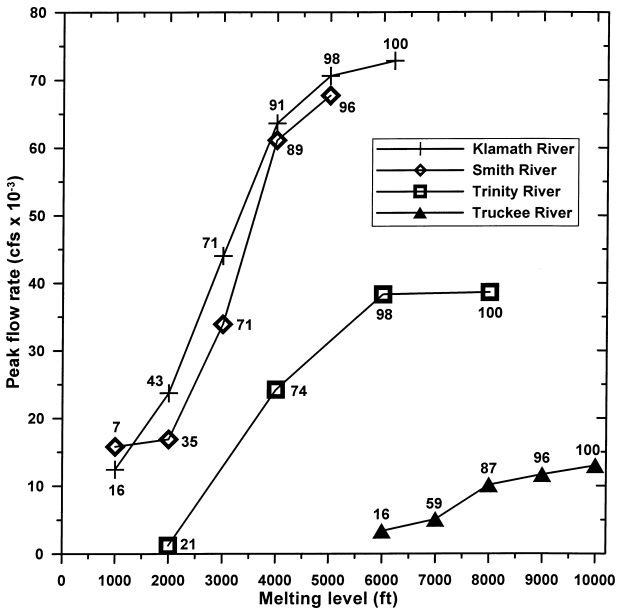

FIG. 3. River forecast model simulations of the sensitivity of runoff to changes in melting level for four river basins in California. The posted numbers give the approximate percentage of basin area below the altitude corresponding to the melting level. These percentages were determined by linearly interpolating the area elevation curves generated for each basin in the SNOW-17 module of the NWSRFS (see text).

The SAC-SMA is a conceptually based soil moisture accounting model. The model distributes soil moisture into upper and lower zones. Within each zone, the moisture is stored as either tension water or free water. The free water can be redistributed within the soil mantle, while the tension water is held by the soil particles and is removed only by evapotranspiration. The movement of water between the upper and lower zones is simulated by a percolation equation, which is controlled by the amount of free water in the upper zone and the moisture deficiency of the lower zone. As the lower-zone storages become full, the capacity for percolation decreases. If there is still water coming into the upper-zone free water, whether it is due to an extended period of rainfall or a burst of intense rainfall, the excess water exits the upper-zone free water into the stream channel in what is called ''interflow.'' The SAC-SMA also simulates runoff from the impervious fraction of the basin. Summarizing, the SAC-SMA converts a certain amount of the rain plus melt applied from the SNOW-17 into runoff. A unit hydrograph operation then converts the runoff into streamflow (Linsley et al. 1982).

The sensitivity of simulated runoff to changes in the melting level for four river basins in California was investigated using the operational version of NWSRFS at the CNRFC. The locations of these basins are shown in Fig. 1. Other relevant information is listed in Table 1. First, each basin was brought to a midwinter soil moisture condition by adjusting the parameters of the SAC-SMA. A 24-h quantitative precipitation forecast (QPF), in 6-h increments, of 0.5, 1.5, 1.5, and 0.5 in., was input into the model. Successive model runs, each using a different melting level ranging from low to high elevations within the basin, were made using this rainfall forecast. The peak streamflow for each run was recorded and plotted as function of melting level in Fig. 3. The increase in runoff with increasing altitude of the snow

level is evident. In some watersheds this increase is very abrupt over a small range of melting levels. For example, in 3 of the 4 watersheds the runoff triples when the melting level rises by 2000 ft. Although the Truckee River basin was the only modeled basin to exceed the flow rate equivalent to flood stage, the input QPF was only modest in strength and duration compared to the more severe climatological events that have occurred in these basins. The results shown in Fig. 3 demonstrate that accurate melting-level information is required to produce a successful river forecast.

3. Brightband characteristics

In precipitation, the DVV provides a reflectivity-weighted, integrated estimate of the fall velocity for the particles distributed within the radar scattering volume during the radar sampling period. A vertical gradient in DVV is associated with the BB because the fall velocity generally increases as snowflakes melt into rain (typically from <2 m s^{-1} for snow to >5 m s^{-1} for rain), which decreases their drag and increases their density. In rain, radar reflectivity factor, Z (m^3), and DVV are usually positively correlated, because larger drops fall faster and increase Z, which is proportional to the drop diameter raised to the sixth power,

$$Z = \int_0^\infty N(D)D^6\, dD, \tag{1}$$

where $N(D)$ is the number concentration (m^{-3}) of drops existing at diameter D (m). The radar equation relates Z to radar reflectivity, η (m^{-1}). For hydrometeors small enough to be considered Raleigh scatterers, the radar equation can be expressed as

$$Z = \frac{\eta\lambda^4}{|K|^2\pi^5}, \tag{2}$$

where λ is the radar wavelength (m), and $|K|$ is the dielectric factor, approximately equal to 0.93 for water and 0.21 for ice. The range-corrected signal-to-noise ratio (SNR) computed from the Doppler radar spectrum is directly proportional to η. The constant of proportionality involves radar constants, operating parameters, and a calibration factor, which depends on the antenna gain and the system noise temperature. To apply our BBH detection algorithm, it is not necessary for the radar to be calibrated, making it possible to apply this algorithm to a wide variety of Doppler radars for which radar calibration may be problematic. Therefore, we can use SNR in place of η.

The upper portion of the BB results as snow or ice particles fall through the melting level and obtain wet surfaces as they begin to melt. This process makes the particles sticky, and aggregation leads to larger particles. Some aggregation may occur above the melting level, as well. As shown in Fig. 2, SNR increases and is positively correlated with DVV in the upper portion of the BB partly because of the increasing particle size. However, SNR increases primarily because $|K|$ is greater for water than for ice (Battan 1973). As the particles undergo further melting their density increases, which leads to larger fall velocities. Hydrodynamically unstable drops break up into smaller drops. This aggregation–break up process has traditionally been used to explain brightband intensity. However, there is still much debate as to whether this effect is important. For example, Fabry and Zawadzki (1995) conclude that shape effects (nonsphericity of melting hydrometeors) contribute more strongly to BB formation at drizzle rates, whereas density effects (related to the way water is distributed within the melting snowflake) are more important at stratiform rain rates. The SNR decreases and is negatively correlated with DVV in the lower portion of the BB because, although the particles are smaller, their fall velocities increase. The SNR also decreases because of the vertical mass flux divergence resulting from the increased fall velocities, which causes $N(D)$ to decrease (Atlas 1964).

4. Brightband height detection algorithm

Because radar reflectivity in the form of range-corrected SNR is used here, the noise profile must be examined for height consistency. In rain the noise power can be artificially enhanced. If the backscatter signal fills or nearly fills the spectral Nyquist interval, the noise power may be enhanced by the tails of the signal. Increased noise power may also result if the signal saturates the receiver. To find the correct noise power, we average the top five range gates of the profile, where the noise is unaffected by these problems. We then recalculate the SNR profile using the average noise power from the top of the profile. This method allows for temporal changes in the noise power that may result from variations in galactic noise or changes in radar hardware performance.

A flowchart describing the steps involved in BBH detection and data quality control via the consensus test is shown in Fig. 4. The first task is to decide whether a subhourly radar SNR–DVV profile pair should be analyzed for a BBH. This step helps eliminate so-called false alarms (i.e., detecting a BBH when a BB does not exist). NOAA's Environmental Technology Laboratory (ETL) deploys a tipping bucket rain gauge with all of its wind profiler installations. One option, then, is to use a rain gauge collocated with the radar to determine when it is raining.[1] This technique was used to produce the BBH measurements during PACJET. Realizing that not all radar sites have rain gauges, we developed a method that relies solely on the radar Doppler spectral moments to determine when to invoke the BBH detection algorithm. The algorithm is applied when at least

[1] The minimum rainfall measurement for the rain gauge referred to in this study is 0.01 in.

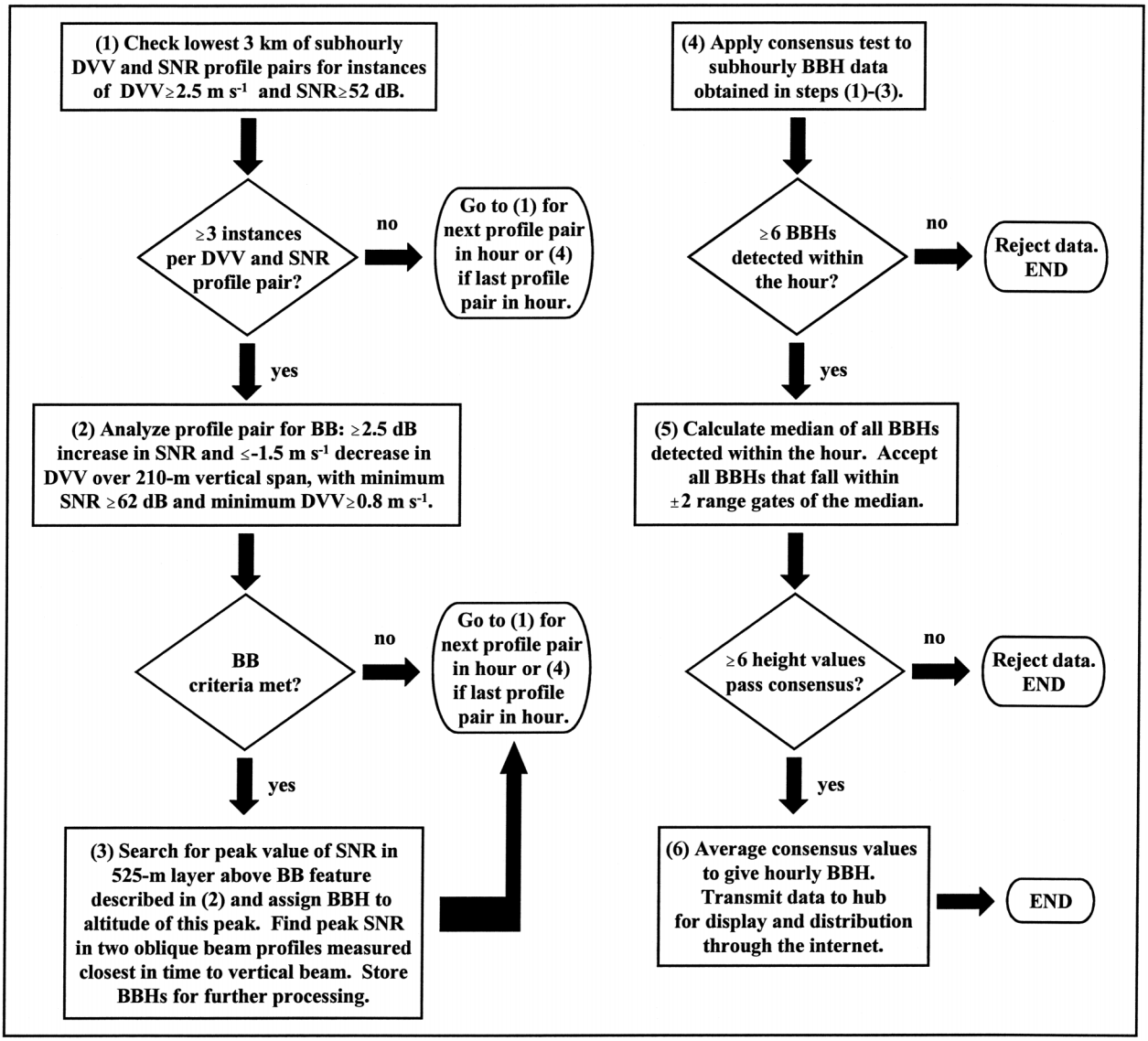

FIG. 4. Flowchart describing a method to deduce the BBH from the DVV and range-corrected SNR profiles recorded by a 915-MHz Doppler wind profiler. Steps (1)–(3) describe the BBH detection algorithm, and steps (4)–(6) describe the consensus test applied to reject outliers and provide a quality-controlled hourly averaged BBH.

3 range gates in the lowest 3 km of the profile measure values of DVV $\geq$ 2.5 m s^{-1} and SNR $\geq$ 52 dB. The SNR threshold is applied to eliminate measurement noise caused by low signal power. The DVV threshold is used to identify profiles that likely contain rain and is based on a study by Ralph et al. (1996) that identified the DVV and SNR characteristics of different types of precipitation.

We evaluated this approach using 915-MHz wind profiler data collected at Bodega Bay, California, during the California Land-falling Jets Experiment (CALJET; Ralph et al. 1999). During CALJET and PACJET, the wind profiler at BBY operated in a Doppler beam swinging mode. The results presented in this study were derived from the 700 ns (105 m) pulse-resolution mode. Typically, the shortest pulse that can be transmitted and detected with the bandwidth available at 915 MHz is 400 ns (60 m). During both experiments, the wind profiler was programmed to sample using three beams: 1 pointing vertically and 2 pointing off-vertically at 75° elevation for CALJET and at 69° for PACJET. Currently, the BBH detection algorithm uses the radar reflectivity measurements from all three beams in addition to the DVV provided by the vertical beam.

As reported in Table 2, this method of determining when to invoke the BBH detection scheme has the advantage of selecting periods for BBH detection when the precipitation does not reach the surface or when the rain rate is insufficient to be detected by a rain gauge. The fact that periods when at least 1 BBH was detected

TABLE 2. BBH detection at BBY during CALJET (Jan–Mar 1998) for hourly periods with and without rainfall observed at the surface.

Bodega Bay, California	Hourly occurrences	Rainfall (mm)
Measurable rain observed	462	818
At least one BBH detected in hour	289 (63%)	607 (74%)
Passed BBH consensus test	242 (52%)	541 (66%)
No measurable rain observed	1698	
At least one BBH detected in hour	95 (6%)	
Passed BBH consensus test	56 (3%)	

accounts for only 74% of the rainfall observed by the rain gauge used in this study is not necessarily an indication that the method underestimates BB occurrence. Orographic precipitation can be generated without the benefit of ice microphysics (i.e., warm rain), which yields reflectivity profiles that do not contain a BB. The warm rain referred to here is a midlatitude, orographically induced, shallow precipitation process that should be differentiated from the convectively driven warm rain process found in the Tropics (Atlas and Ulbrich 2000; Williams et al. 1995; Szoke et al. 1986). In warm rain, collision and coalescence allow cloud droplets to grow into rain drops (Song and Marwitz 1989). This idea was first postulated by Zipser and Lemone (1980). Because this growth process is most efficient when cloud droplets are of different sizes and fall at different speeds, warm rain is more prevalent in coastal regions, where a wide range of aerosol sizes exists (Whiteman 2000). For example, using a vertically pointing 2875-MHz radar ideally suited to BBH detection, White et al. (2001) found that nonbrightband rain accounted for 37% of the total rainfall observed at a coastal mountain site, approximately 35 km from Bodega Bay, California, during the same CALJET period (January–March 1998). This particular 2875-MHz radar, described by White et al. (2000), is better suited to BBH detection than the wind profiler used here because of a selectable microwave coupler that helps prevent receiver saturation in the bright band, continuous vertical profiling, increased sensitivity to hydrometeors, and a narrower beamwidth.

If an SNR–DVV profile pair is selected for BB analysis, the following criteria are used to determine whether a BB exists. Referring to the schematic shown in Fig. 5, the profiles are searched from the bottom up. If an increase in SNR of 2.5 dB and a decrease in DVV of 1.5 m s^{-1} occur over an altitude span of 210 m (three range gates for the radar used in this study), the profile pair is determined to contain a BB, as long as DVV $\geq$ 0.8 m s^{-1} and SNR $\geq$ 62 dB at each of the altitude bounds (i.e., the top and bottom of the shaded region in Fig. 5). If a BB exists, a search is performed to find the peak SNR in the 525-m layer above the altitude at the base of the SNR jump, and the BBH is assigned to the altitude of the peak. Using neighboring range gates in height, or an altitude span of 105 instead of 210 m, required us to use smaller SNR and DVV jump criteria,

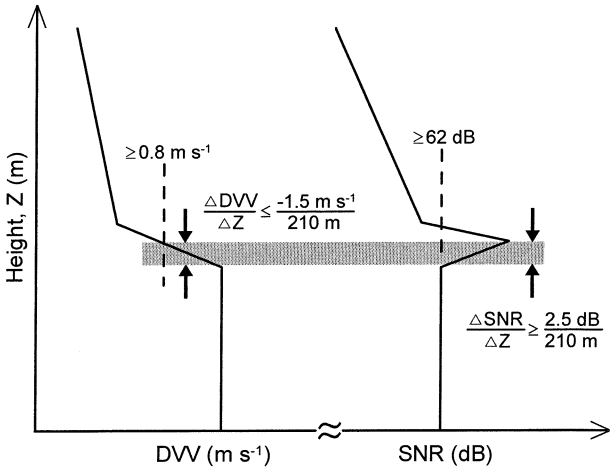

FIG. 5. Schematic showing the classic brightband structure in vertical profiles of DVV (positive downward) and range-corrected SNR. Indicated are the magnitudes of the jumps (denoted by Δs) and thresholds (dashed vertical lines) in DVV and SNR used to detect the lower portion of the bright band (see text).

which increased the number of false alarms. The minimum DVV and SNR thresholds help ensure that some type of precipitation (ice or liquid) is falling and further reduces the chance for false alarms. Note that the SNR threshold we used for precipitation (62 dB) is, coincidentally, an order of magnitude greater than the SNR threshold for noise (52 dB).

If a vertical profile of SNR is determined to have a bright band, the algorithm analyzes the pair of off-ver-

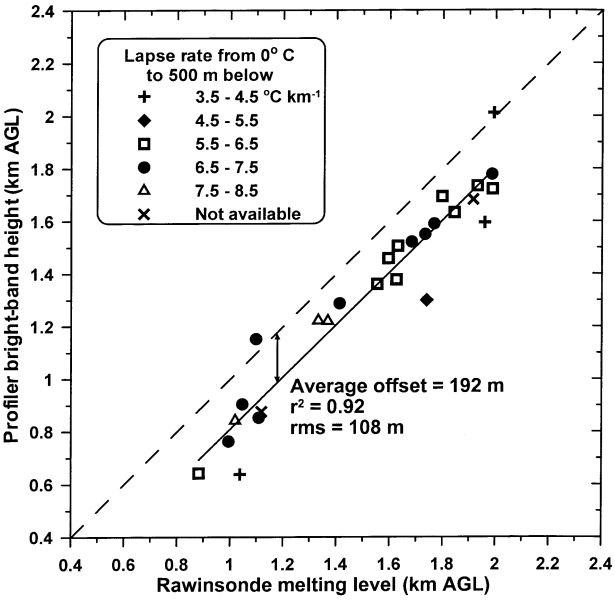

FIG. 6. Comparison of BBH derived from wind profiler Doppler spectral moments with melting levels and temperature lapse rates below the melting levels measured with rawinsondes at Bodega Bay, California, during PACJET. The correlation and average offset are given along with lines of linear regression (solid) and 1:1 agreement (dashed).

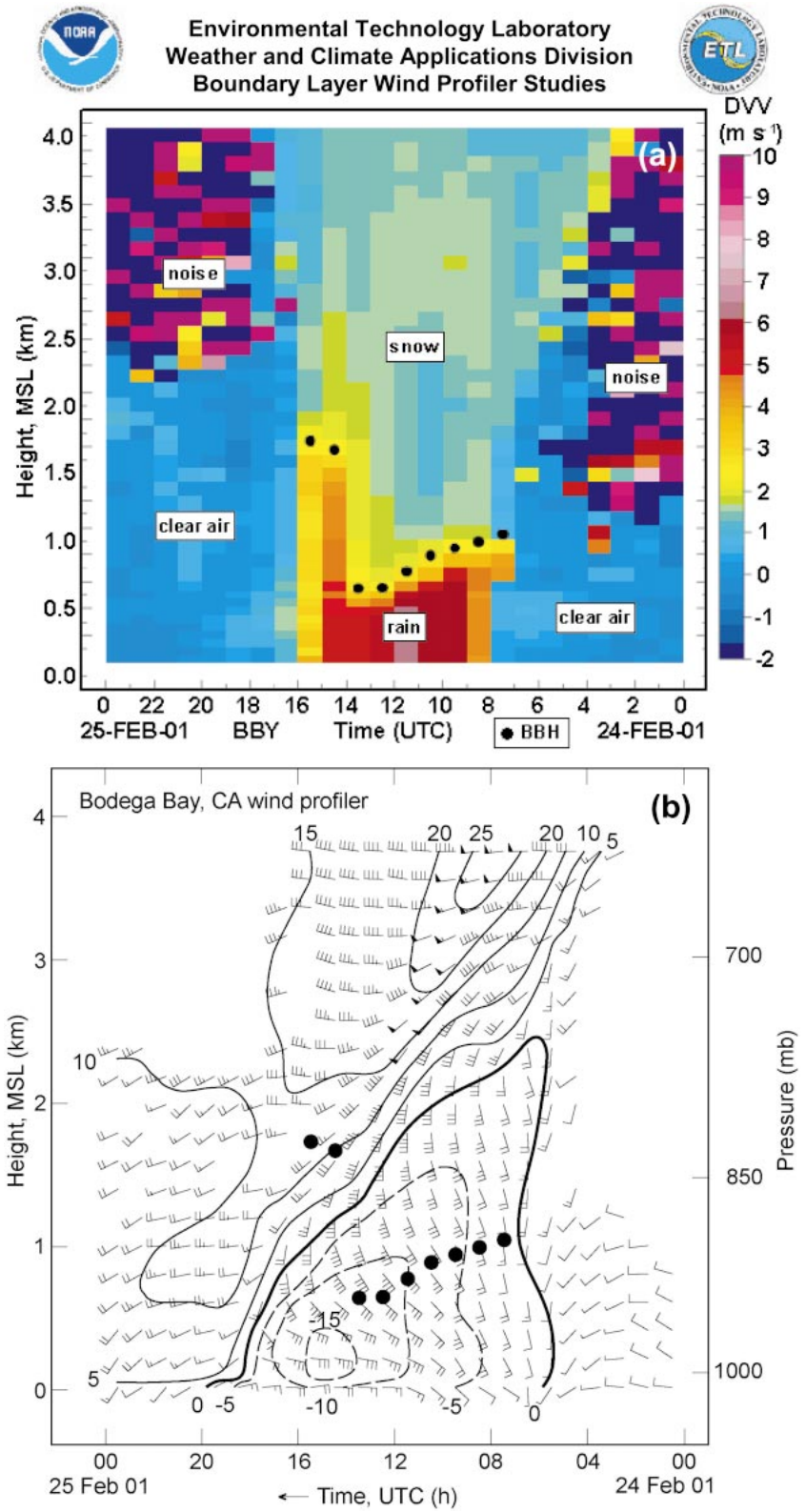
Environmental Technology Laboratory
Weather and Climate Applications Division
Boundary Layer Wind Profiler Studies
DVV
(m s⁻¹)
(a)
noise
snow
noise
clear air
rain
clear air
Height, MSL (km)
Time (UTC)
25-FEB-01
BBY
BBH
24-FEB-01
Bodega Bay, CA wind profiler
(b)
Height, MSL (km)
Pressure (mb)
Time, UTC (h)
25 Feb 01
24 Feb 01

tical beam profiles of SNR measured closest in time to the vertical profile. These profiles are searched for the peak SNR in the 505-m layer (accounting for the slightly different vertical resolution of the off-vertical beams) above the range gate that most closely matches the altitude where the base of the SNR jump occurred in the vertical beam. The addition of BBH data from the off-vertical beams triples the number of samples that otherwise would have been obtained if only the vertical beam had been used, thereby reducing the statistical uncertainty of the average BBHs produced by the consensus method described below.

When applying this method to radars with different sensitivity and/or vertical sampling resolution, the SNR and DVV jump criteria and thresholds should be reevaluated. For other 915-MHz wind proiflers, the SNR and DVV jump criteria as well as the DVV threshold applied here should be valid. The SNR threshold depends not only on the sensitivity of the radar, but also on the Doppler signal processing parameters used to produce the Doppler spectral moments. Specifically, the SNR threshold must be adjusted by the ratio of the number of coherent integrations used with the profiler in question to the number of coherent integrations used with the profiler in this study (160 for CALJET). The fast Fourier transform (FFT) is also a coherent process. Changing the number of FFT points does not affect the SNR directly because the number of FFT points is used in the calculation of noise power. However, the number of FFT points does determine the minimum SNR that can be detected. Therefore, the SNR threshold must also be adjusted by the ratio of the number of FFT points. The Doppler spectral moments from CALJET were produced from spectra generated by 64 FFT points. Because the product formed by the number of coherent integrations and the number of FFT points was the same for CALJET and PACJET, the SNR threshold developed in this study is valid for both experimental datasets.

The BBHs deduced from individual profiles recorded within the hour (up to 24 for the profiler used in this study) are subjected to a consensus test to reject outliers. The test requires that at least six BBHs are detected within the hour. All other cases are thrown out for lack of confidence. For the radar sampling parameters used in this study, this eliminates the possibility of detecting a BBH in rain showers lasting less than about 10 min over the course of a 1-h period. The consensus test consists of establishing a window of acceptable variability and rejecting values that lie outside of the window. To establish the window, a median is computed of all BBHs detected within the hour. Only those heights that fall within 2 range gates above or below the median (a total altitude span of 420 m) are accepted in the consensus. The data for the hour are rejected if less than six BBHs pass this consensus test. Otherwise, an average is computed of all the values accepted in the consensus, and the average is reported as the consensus brightband height (CBBH) for the hour.

As mentioned previously, the BBH is lower than the melting level; that is, the altitude at which the temperature is 0°C. This result is due to the fact that snow can exist several hundred meters below the melting level because of the time required at temperatures above freezing to melt the snow. The distance that snow falls below the melting level depends on the physical properties of the snow particles (shape, size, density) as well as the temperature and humidity profiles, the ambient vertical velocity, and the precipitation rate. During PACJET, BBHs were computed using subhourly radar SNR and DVV profile pairs measured with the 915-MHz wind profiler at Bodega Bay, California. In Fig. 6, CBBHs are compared to the melting levels and temperature lapse rates below the melting levels measured by serial rawinsondes launched from the same location. A total of 56 rawinsondes penetrated the melting level, and an hourly CBBH was detected in the hour surrounding the melting-level measurement time in 27 of these cases. These soundings were taken in the variety of synoptic conditions characteristic of the land-falling winter storms that affect the Pacific Coast each winter. Keeping in mind that the rainfall rates at the coast can be significantly lower than the rainfall rates observed in the coastal mountains (Neiman et al. 2002), the rainfall rates measured in the hour surrounding the melting level measurement time ranged from 0.0 to 10.4 mm h^{-1}. The maximum 1-min rainfall measured was 1.524 mm, corresponding to an hourly rate of 91.4 mm h^{-1}. Of the 27 cases shown in Fig. 6, 11 had rain rates of 1.0 mm h^{-1} or less. On average, the CBBHs were 192 m lower than the melting levels measured by the rawinsondes. This particular result is specific to the location where the measurements were obtained (coastal California) and the winter season that was analyzed in part (January–February 2001). However, Fig. 6 is sufficient to demonstrate that the BBH approximates the snow level.

←

FIG. 7. (a) Example of a BBH image from PACJET displayed on a real-time data Web site (http://www7.etl.noaa.gov/data/). The colored rectangles display hourly averaged values of DVV, (positive downward) recorded by the wind profiler at BBY (elev 12 m) on 24 Feb 2001. The BBH data are indicated by black dots. The time axis proceeds from right to left. Heights are MSL. The image has been annotated to indicate patterns of DVV corresponding to radar backscatter from different atmospheric media. Noise refers to measurement noise caused by low signal power. (b) Time–height cross section of wind barbs (flag = 25 m s^{-1}; full barb = 5 m s^{-1}; half barb = 2.5 m s^{-1}) and isotachs (m s^{-1}) of the zonal wind component recorded by the wind profiler at BBY for the same period as in (a). The descending warm front is dilineated by a region of enhanced speed and directional wind shear. The black dots are the same BBHs plotted in (a).

5. Implementation

In order for BBH measurements discussed in this paper to be of value, the information must be made available to end users in a timely manner. The following is a brief description of how this goal was achieved during PACJET. Accessing the wind profiler Doppler spectral moments to use as input for the BBH detection algorithm requires I/O synchronization with the radar control program since new data is actively acquired and written to the file archive with exclusive access rights by the radar control program.[2] The time between disk writes was used, therefore, to access the necessary data. After the radar data was accessed and stored on disk, the BBH detection program was spawned by a process control routine. The resulting BBH output data files were then transferred back to a central data hub via phone lines. Once the BBH data files were received, graphical images of contoured DVV and BBH were created and made available on the Internet. During PACJET, the posting of the hourly BBH images occurred 30–40 min after the top of each hour. An example taken with the wind profiler at Bodega Bay, California, during PACJET is shown in Fig. 7a.

The profiler deduced BBHs from 0900 to 1400 UTC depict cooling in the lower troposphere caused by offshore flow (i.e., flow with an easterly component), as shown in Fig. 7b. The subsequent rapid increase in BBH resulted as a warm front passed over the wind profiler site, as identified by the descending region of enhanced zonal wind shear and the shift from offshore to onshore flow (i.e., flow with a westerly component) also evident in Fig. 7b. This example demonstrates, at least for this case, that hourly retrieved BBH measurements are adequate for looking at changes in the melting level associated with synoptic-scale fronts.

6. Summary

We demonstrated an algorithm for detecting the brightband height in vertical profiles of Doppler vertical velocity and radar reflectivity recorded by a Doppler wind profiler and distributing results through the internet in near–real time. The brightband height provides a better estimate of the snow level than the melting level because of the time required for snow to melt at temperatures above freezing. The brightband height detection algorithm described here can be applied to a wide variety of operational and research Doppler radars and, thus, has the potential to benefit a large number of individuals and organizations who require information about the snow level. A detailed illustration of this was provided in terms of streamflow forecasts using the NWS operational hydrological model. In 3 out of 4 watersheds examined, a 2000-ft rise in the melting level caused a tripling of runoff. The benefit of providing brightband height measurements in real time will be evaluated at approximately 10 wind profiler sites in California during the second phase of the Pacific Land-falling Jets Experiment scheduled to take place during the 2001/02 winter season.

Acknowledgments. We thank all the scientists who contributed to the success of the California Land-falling Jets Experiment (CALJET) and Pacific Land-falling Jets Experiment (PACJET). Special thanks to David White (CIRES/NOAA/ETL) and Dan Wolfe of (NOAA/ETL) for deploying and operating the GPS rawinsonde systems during PACJET; and Scott Abbott, Clark King, Jesse Leach (all NOAA/ETL), and Dave Costa (CIRES/NOAA/ETL) for deploying and maintaining the wind profiler at Bodega Bay during CALJET and PACJET. CALJET and PACJET were sponsored by NOAA. The comments provided by three anonymous reviewers helped to improve this manuscript.

[2] At the time of publication, the NOAA/ETL wind profilers were operated with the LAP-XM℠ radar control and data acquisition software.

REFERENCES

Anderson, E. A., 1973: National Weather Service River Forecast System—Snow Accumulation and Ablation Model. NOAA Tech. Memo. NWS HYDRO-17, 217 pp.

Atlas, D., 1964: Advances in radar meteorology. *Advances in Geophysics*, Vol. 10, Academic Press, 317–478.

——, and C. W. Ulbrich, 2000: An observationally based conceptual model of warm oceanic convective rain in the Tropics. *J. Appl. Meteor.*, **39,** 2165–2181.

Battan, L. J., 1973: *Radar Observations of the Atmosphere*. University of Chicago Press, 279 pp.

Burnash, R. J. C., R. L. Ferral, and R. A. McGuire, 1973: A generalized streamflow simulation system—Conceptual modeling for digital computers. National Weather Service and California Dept. of Water Resources, 204 pp.

Burrows, D., 2001: An operational algorithm for the identification and location of a bright band from radar volume data. Preprints, *30th Int. Conf. on Radar Meteorology*, Munich, Germany, Amer. Meteor. Soc., 587–588.

Ecklund, W. L., D. A. Carter, and B. B. Balsley, 1988: A UHF wind profiler for the boundary layer: Brief description and initial results. *J. Atmos. Oceanic Technol.,* **5,** 432–441.

Fabry, F., and I. Zawadzki, 1995: Long-term radar observations of the melting layer of precipitation and their interpretation. *J. Atmos. Sci.,* **52,** 838–851.

Glickman, T. S., Ed., 2000: *Glossary of Meteorology*. 2d ed. Amer. Meteor. Soc., 855 pp.

Gourley, J. J., J. Zhang, R. A. Maddox, C. M. Calvert, and K. W. Howard, 2001: A real-time precipitation monitoring algorithm—Quantitative precipitation estimation and segregation using multiple sensors (QPE SUMS). Preprints, *Symp. on Precipitation Extremes: Prediction, Impacts, and Responses*, Albuquerque, NM, Amer. Meteor. Soc., 57–60.

Linsley, R. K., M. A. Koher, and J. L. H. Paulhus, 1982: *Hydrology for Engineers.* 3d ed. McGraw-Hill, 508 pp.

Neiman, P. J., F. M. Ralph, A. B. White, D. E. Kingsmill, and P. O. G. Persson, 2002: The statistical relationship between upslope flow and rainfall in California's coastal mountains: Observations during CALJET. *Mon. Wea. Rev.*, 1468–1494.

Ralph, F. M., P. J. Neiman, and D. Ruffieux, 1996: Precipitation identification from radar wind profiler spectral moment data: Vertical velocity histograms, velocity variance, and signal pow-

er-vertical velocity correlations. *J. Atmos. Oceanic Technol.,* **13,** 545–559.

——, and Coauthors, 1999: The California Land-falling Jets Experiment (CALJET): Objectives and design of a coastal atmosphere–ocean observing system deployed during a strong El Niño. Preprints, *Third Symp. on Integrated Observing Systems,* Dallas, TX, Amer. Meteor. Soc., 78–81.

Smith, C. J., 1983: The reduction of errors caused by bright band in quantitative rainfall measurements made using radar. Part I: Detection of bright bands in real-time. Met Office Radar Research Laboratory Res. Rep. 38, Met Office, Malvern, United Kingdom, 25 pp.

Smith, G. F., and D. Page, 1993: Interactive forecasting with the National Weather Service River Forecast System. Preprints, *Third National Technology Transfer Conf.,* Vol. 1, Baltimore, MD, NASA Conf. Publ. 3189, 527–536.

Song, N., and J. Marwitz, 1989: A numerical study of the warm rain process in orographic clouds. *J. Atmos. Sci.,* **46,** 3479–3486.

Szoke, E. J., E. J. Zipser, and D. P. Jorgensen, 1986: A radar study of convective cells in mesoscale systems in GATE. Part I: Vertical profile statistics and comparison with hurricanes. *J. Atmos. Sci.,* **43,** 182–197.

White, A. B., C. W. Fairall, A. S. Frisch, B. W. Orr, and J. B. Snider, 1996: Recent radar measurements of turbulence and microphysical parameters in marine boundary layer clouds. *Atmos. Res.,* **40,** 177–221.

——, J. R. Jordan, B. E. Martner, F. M. Ralph, and B. W. Bartram, 2000: Extending the dynamic range of an S-band radar for cloud and precipitation studies. *J. Atmos. Oceanic Technol.,* **17,** 1226–1234.

——, F. M. Ralph, P. J. Neiman, D. A. Kingsmill, and P. O. G. Persson, 2001: Process partitioning of rainfall enhanced by coastal orography. Preprints, *Symp. on Precipitation Extremes: Prediction, Impacts and Responses,* Albuquerque, NM, Amer. Meteor. Soc., 8–11.

Whiteman, C. D., 2000: *Mountain Meteorology: Fundamentals and Applications.* Oxford University Press, 355 pp.

Wilczak, J. M., and Coauthors, 1995: Contamination of wind profiler data by migrating birds: Characteristics of corrupted data and potential solutions. *J. Atmos. Oceanic Technol.,* **12,** 449–467.

Williams, C. R., W. L. Ecklund, and K. S. Gage, 1995: Classification of precipitating clouds in the Tropics using 915-MHz wind profilers. *J. Atmos. Oceanic Technol.,* **12,** 996–1012.

Zipser, E. J., and M. A. LeMone, 1980: Cumulonimbus vertical velocity events in GATE. Part II: Synthesis and model core structure. *J. Atmos. Sci.,* **37,** 2458–2469.